

Time-Resolved X-ray Diffraction of Biological Materials

SOL M. GRUNER

Instrumental and specimen considerations pertinent to performing time-resolved x-ray diffraction on biological materials are discussed. Existing synchrotron x-ray sources, in conjunction with integrating x-ray detectors, have made millisecond diffraction experiments feasible; exposure times several orders of magnitude shorter than this will be possible with synchrotron sources now on the drawing boards. Experience gained from time-resolved studies together with order-of-magnitude estimates of specimen requirements can be used to determine the instrumental capabilities needed for various time-resolved experiments. Existing instrumental capabilities and methods of dealing with time-resolved specimens are reviewed.

X-RAY DIFFRACTION TECHNIQUES HAVE TRADITIONALLY been limited to probing the structure of static materials simply because the time required to collect the diffraction data has typically been hours or days. Within the last decade, however, the development of intense x-ray sources, efficient data collection methods, and new x-ray detectors has reduced the data acquisition times, for many materials, to milliseconds, thereby allowing the examination of rapidly changing structures. The purpose of this article is to survey the instrumental requirements of time resolved x-ray diffraction, especially as they pertain to biological materials. The spirit of the article is to combine order of magnitude estimates and experience derived from representative studies to illustrate time-resolved experiments that are being performed or will be possible in the near future.

The requirements of time-resolved diffraction constrain each of the three major components of a diffraction experiment: the x-ray source, the specimen, and the x-ray detector. The source intensity, spectrum, and beam divergence characteristics must be sufficient to produce acceptable signal-to-noise ratios in a well-resolved diffraction pattern within the time constraints imposed by the specimen. The specimen lattice and orientation relative to the x-ray beam should ideally be such that a large part of the reciprocal lattice meets the diffraction condition. The specimen also requires a trigger that initiates a structural change that evolves uniformly throughout the specimen. Finally, the x-ray detector must be able to rapidly record and store the diffraction pattern with acceptable levels of noise and efficiency.

The availability of intense storage ring, or synchrotron, x-ray sources (I) has stimulated development of x-ray beam lines, specimen triggering and analysis methods, and advanced x-ray detectors.

This is shown in Table 1, which lists some representative (2) time-resolved studies that have been performed on biological materials.

X-ray Sources

Most time-resolved diffraction experiments have been small-angle x-ray scattering (SAXS) studies of noncrystalline substances (Table 1). Although the scattering power of such specimens varies widely, most biological specimens have an x-ray scattering power, S , that falls in the range $10^{-3} < S < 10^{-6}$ for x-rays of wavelength $\lambda \approx 1.5$ Å. For our purposes, S may be defined as the number of diffracted x-ray photons scattered into a typical area detector (per unit time) divided by the number of x-ray photons incident upon the specimen. Given such scattering powers, one can estimate the time required to perform SAXS experiments at various x-ray sources. First, consider a conventional rotating-anode x-ray source coupled to small-angle x-ray optics, such as a Franks camera (3) or mirror-monochromator camera (4). If one is careful, such arrangements yield x-ray intensities, I , incident upon a 1 mm² cross-sectional area of the specimen of between 10^6 and 10^8 photons per second. The number of x-ray photons per second diffracted into an area detector is, then, just the product of the incident intensity and the scattering power, $S \times I$. Now assume, for the sake of illustration, that the diffraction pattern is to be integrated into 100 areas, or channels, of interest; each area might, for instance, be a Bragg reflection. Although the diffracted intensity per channel generally varies widely across a given diffraction pattern, it may be assumed that the relative intensities in different channels fall within the four orders of magnitude variation of S . Hence, taking extreme values of S and I , the diffracted intensity is in the range of $10^{-2} < (S \times I)/100 < 10^3$ photons per second per channel. Finally, assume one wishes to measure each channel to 3% accuracy and that one is using a quantum-limited area detector. In this ideal case, the signal-to-noise ratio is dominated by the Poisson statistics of the diffraction pattern incident on the detector. To achieve 3% accuracy, each channel must receive roughly 10^3 x-rays [that is, accuracy = noise/signal = $(1000)^{1/2}/1000 \approx 3\%$]. So, the integration time per channel is simply $1 < 10^3/[(S \times I)/100] < 10^5$ seconds.

The above argument indicates that x-ray exposure times for biological materials typically vary from a second or so to several days at conventional x-ray sources. This agrees well with experience. Useful SAXS diffraction patterns are routinely obtained in a few seconds for strongly diffracting phospholipid liquid crystals on the area detectors in our laboratory. On the other hand, several days of exposure are not uncommon for weakly scattering protein solutions or for the higher orders of poorly organized biomembrane multilayers or muscle.

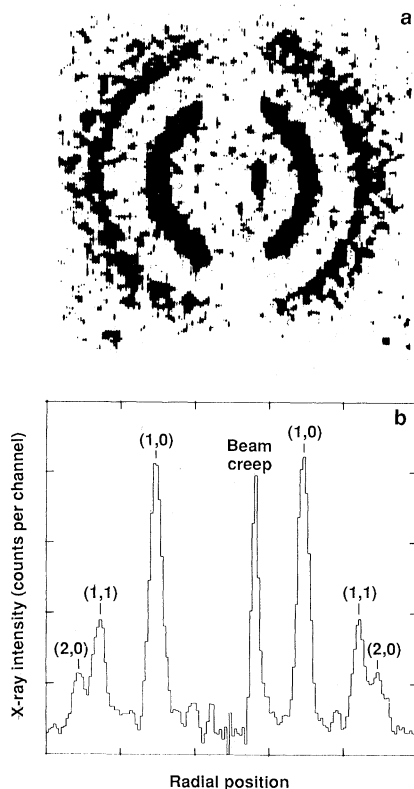
To compute exposure times at synchrotron x-ray sources, note that exposure times scale inversely with the incident x-ray flux.

The author is associate professor of physics at Princeton University, Princeton, NJ 08544.

Bending-magnet beam lines at high intensity rings, such as the Cornell High Energy Synchrotron Source (CHESS) at Cornell University (5) or the National Synchrotron Light Source (NSLS) at Brookhaven National Laboratory (6), yield $10^{10} < I < 10^{12}$ photons per second per square millimeter of highly monochromatic radiation at the specimen. Repeating the calculations described above yields exposure times of 10^{-4} to 1 second. Millisecond diffraction is readily obtainable for many specimens. Indeed, exposures of 10 msec have been used for several studies, as shown in Table 1. (The exposure times listed in Table 1 generally exceed the minimum times that were required to obtain data to the desired accuracy. Investigators conservatively choose exposure times based on considerations of the strength of the diffraction, the time scale of the process being studied, and limitations of the instrumentation.)

An example of a 12-msec diffraction pattern obtained at the NSLS with an unoriented hexagonal phase phospholipid-water dispersion is shown in Fig. 1 (7). The goal of the experiment was to determine

Fig. 1. (a) A 12-msec small angle diffraction pattern of an inverse hexagonal phase phospholipid-water liquid crystal. This pattern was recorded at the NSLS on beam line X-10 on a slow-scan TV-based x-ray detector (25). The pattern shown here was made by synthesizing the digital data array into a gray scale image on a TV monitor, which was then photographed with high contrast film. The pattern is x-ray quantum limited; this accounts for its "graininess." **(b)** X-ray intensity after radial integration. The peaks resulting from the hexagonal lattice, indexed as (h, k) , are easily seen. The central peak is an edge of the incident beam creeping around the beam stop. The radial position is in arbitrary distance units from the center of the diffraction pattern.



the phase and unit-cell dimensions of the lipid dispersion after a rapid, ohmically induced temperature jump. These parameters are easily determined from Fig. 1. The limiting 12-msec exposure time of Fig. 1 was set by the aperture time of a mechanical x-ray shutter. The integrated signal from some of the lipid samples examined was sufficiently intense that, had a faster x-ray shutter been installed, 3% accuracies could have been obtained in a few hundred microseconds. In fact, longer exposures were used for most of the experiment because the time scale of changes within the specimens was tens of milliseconds.

Considerably shorter exposure times are, of course, possible with higher x-ray fluxes. The values of 10^{10} to 10^{12} photons per second per square millimeter assumed above are obtained with dipole bending magnets and crystal monochromators at existing synchrotron rings. At a bending-magnet beam line, the trajectory of a highly relativistic electron beam is deflected by a dipolar magnetic field. Electron storage rings consist, in fact, of straight segments linked by dipole bending magnets; synchrotron radiation is a consequence of the radial acceleration imposed on the electrons by the bending magnets. The electrons may also be made to undergo a series of closely spaced oscillations, that is, multiple accelerations, by enclosing a straight section of the electron path with a series of closely spaced, alternating magnetic fields. These radiation-enhancing devices, descriptively called wigglers and undulators (1, 8), are collectively known as insertion devices because they are inserted in the straight paths of the electron beam.

Bending magnets and many insertion devices produce a continuum of radiation wavelengths known as white radiation. Highly monochromatic radiation of wavelength λ , with a bandpass $\Delta\lambda/\lambda \approx 10^{-4}$ is typically selected by orienting a silicon or germanium crystal in the white beam at an angle θ such that a diffracted ray meets the Bragg condition, $\lambda = 2d\sin\theta$, where d is the lattice spacing of the crystal and 2θ is the scattering angle. For many SAXS studies, such a high degree of monochromatization is not required and a considerable flux enhancement results from passing a wider slice of the white beam. Techniques for widening the bandpass include absorption-edge filters, membrane mirrors, mosaic crystals, and layered synthetic microstructures (9). At existing sources, white beam intensities at the specimen of 10^{14} to 10^{16} photons per second per square millimeter are obtainable (10). Additional enhancement in flux over existing sources would be available with insertion devices at the 5- to 6-GeV rings planned for the European Synchrotron Research Facility or the Advanced Photon Source being planned for the Argonne National Laboratory in Illinois (11).

With incident intensities of 10^{15} photons per second per square

Table 1. Representative time-resolved x-ray diffraction studies of biological materials.

Material	Exposure time (msec)	X-ray* source	Trigger	Detector†	Reference
Muscle	10	DESY	Electrical and mechanical	1-D wire	(18)
Muscle	100	DESY	Electrical	2-D TV	(38)
Sarcoplasmic reticulum membrane	200	SSRL	Caged ATP	2-D TV	(16)
Purple membrane	10^{-6}	Laser UR-LLE	Light	2-D TV	(13)
Lipids	10	NSLS	Temperature	2-D TV	(7)
Lipids	30 to 500	CHESS	Temperature	2-D TV	(15)
Collagen fibril solution	5,000	DESY	Temperature	1-D wire	(39)
Tubulin	15,000	DESY	Temperature	1-D wire	(40)
DNA	4 to 10 minutes	SRS	Relative humidity	Film	(41)
Protein crystals (Laue)	4 to 30,000	CHESS	(Static)‡	Film	(9, 21)

*Except for the laser source, described in the text, these are all synchrotron storage rings. See (42) for a worldwide census of synchrotron sources. Abbreviations: DESY, Deutsches Elektronen Synchrotron, Hamburg, West Germany; SSRL, Stanford Synchrotron Radiation Laboratory; Laser UR-LLE; Laser Source at the University of Rochester Laboratory for Laser Energetics; NSLS, National Synchrotron Light Source, Brookhaven National Laboratory; CHESS, Cornell High Energy Synchrotron Source; SRS, Synchrotron Radiation Source, Daresbury, United Kingdom. †Abbreviations: 1-D wire, one-dimensional wire counter; 2-D TV, two-dimensional TV detector. ‡These were feasibility studies done on static crystals.

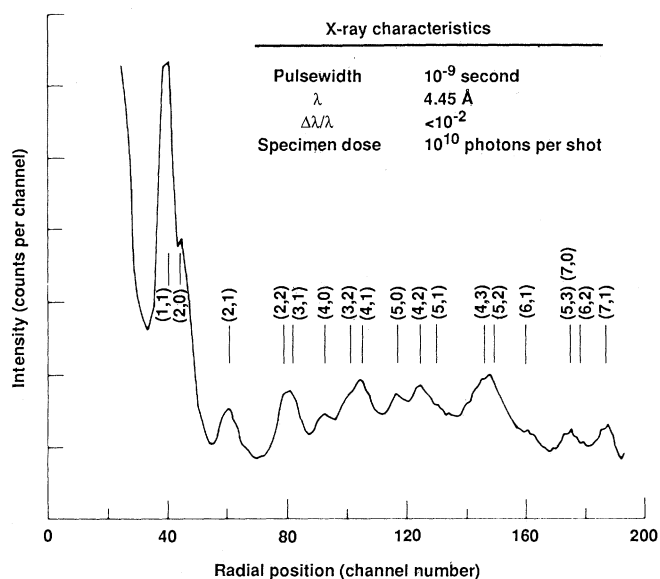


Fig. 2. A circular average through the two-dimensional diffraction pattern of a 1-nsec exposure of a powder of dried purple membrane. The x-rays were generated with the laser-driven x-ray source at the University of Rochester Laboratory for Laser Energetics. The positions and (h, k) indices of the in-plane hexagonal lattice of purple membrane are indicated. The abscissa is in arbitrary units of detector channels from the center of the diffraction pattern, and the ordinate is in counts per channel. The two-dimensional diffraction pattern was recorded on an integrating TV-based detector. [Reproduced from (13) with permission of the Biophysical Society]

millimeter, exposure times on biological materials shrink to 10^{-7} to 10^{-4} second. At such x-ray intensities, specimen heating and radiation damage become severely limiting. At x-ray wavelengths of $\sim 1.5 \text{ \AA}$ typical organic materials, or water, absorb roughly a factor of $(1 - e^{-1})$ of the x-rays incident upon a 1-mm path length of sample. At 10^{15} photons per second per square millimeter, a specimen 1 mm on a side would absorb almost 0.8 W of power, corresponding to an adiabatic temperature rise of about $190^\circ\text{C}/\text{sec}$; faster temperature rises occur if the x-rays are focused onto a smaller spot. At very high flux all biological diffraction requires, of necessity, very short exposure times (12).

Nonthermal radiation damage is more difficult to estimate because little is known about the details of radiation damage, because specimens vary with respect to radiation damage susceptibility, and, most importantly, because changes in the magnitude of damage with dose rate, as opposed to dose, are not well understood. A rough estimate of the problem for protein samples may be obtained by assuming that the number of damaged proteins per absorbed x-ray ranges from approximately 1 to 100 (12). Then a 1-mm³ specimen whose mass is half water and half protein (of 50-kilodalton mass, for example), contains about 5×10^{15} molecules. At 10^{15} photons per second per square millimeter, the time to absorb 5×10^{15} x-rays, sufficiently to damage, on the average, each protein, is 0.08 to 8 seconds.

On the basis of experiments with microcrystals of protein, Hedman *et al.* (10) estimated that standard-size protein crystals would survive a beam of 10^{13} to 10^{14} photons per second per square millimeter, for about a minute before major radiation damage occurs, consistent with the order of magnitude estimate computed above. Detailed calculations of heating and radiation damage for protein crystals under a variety of synchrotron radiation situations are given by Helliwell and Fourme (12).

The only experiment listed in Table 1 that did not use synchrotron radiation was the purple membrane study of Frankel and Forsyth (13), which involved the laser x-ray source installed at the

Laboratory for Laser Energetics at the University of Rochester. X-rays were generated by focusing a high power laser, of the type used for laser fusion studies, onto a chlorine-containing target. The resulting plasma, in which a chlorine line was excited, emitted 4.45- \AA x-rays from a 100- μm -diameter spot for roughly 1 nsec. The focused flux on the specimen was approximately 10^{10} x-rays per shot, which allowed nanosecond exposures of purple membrane specimens (Fig. 2). The drawbacks of the laser source are availability (only one facility exists), the limited number of x-rays per shot, and the repetition rate of a few shots per hour.

The time structure of synchrotron radiation also can be used for nanosecond resolution. Synchrotron radiation is actually emitted in nanosecond-long pulses several million times a second. This is a consequence of the fact that the circulating electrons in the storage ring are grouped in "bunches" each about 3 to 30 cm long; a pulse of radiation 0.1 to 1 nsec in duration (τ') is emitted each time a bunch traverses a bending magnet or insertion device. The pulsed nature of the radiation may be used to advantage for rapid time resolution studies. Suppose one is examining a biological process that may be repetitively cycled many times and that may be triggered rapidly. An example might be observation of structural changes that are triggered by a nanosecond laser pulse in a reversible, photosensitive protein. Suppose, further, that the excited state of the protein has a lifetime less than the period between successive bunches. Then to examine the state of the protein τ nanoseconds after excitation, one synchronizes the excitation laser pulse to the circulating electrons so that the laser pulse excites the specimen τ nanoseconds before arrival of each bunch at the x-ray beam port. X-ray exposure will then always occur between the τ and $\tau + \tau'$ nanosecond after laser excitation. An x-ray detector integrates the signal from as many excitations and bunches as required to obtain good signal statistics. The entire time course of the event is obtained by systematically varying the delay time τ . Although this technique has yet to be applied to biological diffraction, it has been used by Larson *et al.* (14) to measure temperature gradients in silicon during pulsed laser annealing.

Specimens

Specimens must meet certain constraints if they are to be suitable for time-resolved x-ray diffraction:

1) The dynamical process must have a well-defined trigger to set the time at $t = 0$. Once triggered, all the diffracting units within the sample should, ideally, evolve at nearly the same rate.

2) The generalized reciprocal lattice of the specimen and the Ewald sphere of reflection must have suitable overlap during the dynamical process. This is called "meeting the diffraction condition."

3) The specimen must yield useful x-ray signal statistics. This is largely a function of the source intensity and diffracting power of the specimen, as has already been discussed.

4) The specimen must survive sufficiently long after triggering that adequate data can be collected. For example, the lattice of a protein crystal may change and cause the crystal to crack upon initiation of a dynamic event.

Triggers

Dynamical processes in biological materials are typically triggered by a variety of stimuli, including changes in temperature, applied force, chemical concentration, light, applied voltage, and pressure (column 4 of Table 1). The most commonly used trigger is a change

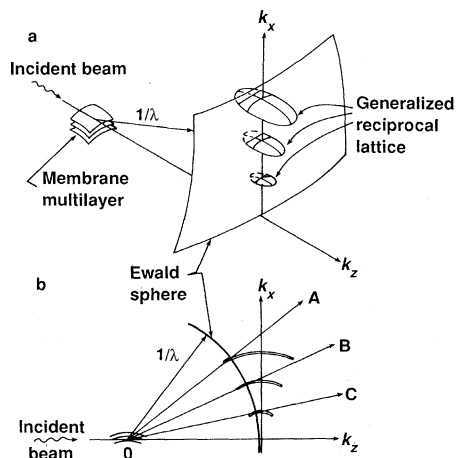


Fig. 3. The generalized reciprocal lattice from a membrane multilayer paracrystal intersecting a section of the Ewald sphere is shown (a) in three dimensions and (b) in cross section in the $k_x - k_z$ plane of reciprocal space. If the membranes were all equidistant from one another, and perfectly parallel to the k_z axis, the reciprocal lattice would be a series of equally spaced points on the k_x axis; waviness in the multilayer (for example, "mosaic spread") effectively spreads the reciprocal lattice points into a distribution called the generalized reciprocal lattice, that is, the ensemble average of all tilts of the ideal lattices corresponding to each tilted section of the multilayer. The diffraction condition (Bragg's law) is met whenever the generalized reciprocal lattice intersects the Ewald sphere. For example, diffraction simultaneously occurs along directions represented by rays OA, OB, and OC.

in ambient temperature. Although large, rapid temperature jumps are readily achieved by laser pulses or by electrical discharges, small, reproducible, and rapid temperature jumps in bulk samples are, in fact, hard to achieve. Consider, for example, how one might rapidly increase the temperature of a biological specimen 1 mm on a side by 10°C . If the thermal characteristics of the materials are approximately those of water, which is often true for biological substances, then an energy of 40 mJ is required to make the temperature jump. How might such a temperature jump be performed? The simplest way, thermal conduction, is slow: Imagine suddenly placing two metal walls at temperature $T + 10^\circ\text{C}$ against opposite sides of a specimen 1 mm on a side and initially at temperature T . The initial heat flow rate will be $\approx 2\sigma A\Delta T/L$, where σ is the thermal conductivity of the specimen, the area A is 1 mm^2 , $\Delta T = 10^\circ\text{C}$, and the thermal depth is $L \approx 0.5\text{ mm}$. If σ is approximately that of water ($\sim 6\text{ mJ sec}^{-1}\text{ cm}^{-1}\text{ K}^{-1}$), then the initial heat flow rate is about 20 mJ/sec. Even if this initial rate were maintained, and it will not be as ΔT decreases, 2 seconds would be required to heat the specimen. Other problems with this approach are thermal gradients through the specimen and a nonuniform heating rate. A more realistic strategy that avoids at least some of these problems is to regulate the flow of heat into the specimen. Caffrey [Table 1 and (15)] did this for lipid dispersions by using a laminar flow of hot air past an x-ray capillary. The result was a nearly uniform heating rate of the specimen, the diffraction of which was recorded continuously by means of a vidicon-type x-ray detector. However, heating of the capillary still required many seconds.

The limitations of heat conduction arise from the fact that it is driven by a thermal gradient across an interface. Bulk heating methods are, in general, preferable because thermal gradients are avoided. For example, heating may be performed by microwave or optical radiation. In the former case, extraordinary, but not impossible, microwave power densities are needed for millisecond jumps of tens of degrees. Laser heating is more tractable, although care must be taken to make the specimen mostly transparent to the heating radiation if thermal gradients are to be avoided. Another method is to use ohmic heating by passing an electrical current through the

specimen. This method was used by Tate *et al.* [Table 1 and (7)] in examining the phase transition behavior of lipid-water dispersions. For the sake of illustration, assume the specimen is 25% physiological saline solution. Then the resistance of a specimen 1 mm on a side is about $R = 4$ kilohms. The power needed to raise the temperature by 10°C in 1 msec is $P = 40\text{ mJ/msec} = 40\text{ W}$. This requires a voltage, $V = (PR)^{1/2} \approx 400\text{ V}$, across the specimen. Pitfalls of the ohmic heating method include electrical breakdown and gas generation at the electrodes. These problems are somewhat minimized by the use of ac current and by simultaneous current and voltage regulation of the power source so as to smoothly program the flow of power into the specimen.

Changes in chemical concentration are important triggers, especially in so far as they simulate initiators of *in vivo* biological processes. Sudden changes in the ambient concentration of a chemical are difficult to achieve because of slow diffusion gradients similar to those encountered with thermal gradients. A clever way of initiating a bulk change in chemical concentration is to use a photolabile substrate cage. For example, Blasic *et al.* [Table 1 and (16)] used a caged adenosine 5'-triphosphate [ATP; (17)] to examine changes in sarcoplasmic reticulum membrane multilayers upon stimulation with free ATP. The ATP cage covalently binds ATP in a catalytically inert form until hit by a pulse of ultraviolet light, whereupon the ATP is released. For this experiment, the multilayer was saturated with the caged ATP before photostimulation. Since adenosine 5'-diphosphate (ADP) does not stimulate the sarcoplasmic reticulum ATPase, a caged ADP served as a control against heating artifacts.

Other triggers include light, applied voltage, mechanical stimulation, and pressure. Laser light flashes were used to stimulate the photosensitive bacteriorhodopsin membranes examined in the Franke and Forsyth study [Table 1 and (13)]. Voltage triggers and mechanical stimuli were used to stimulate the muscles in the classic studies of muscle contraction performed by Huxley and colleagues [Table 1 and (18)]. Many biological samples are sensitive to pressure. Pressure jumps have not yet been extensively used for time-resolved diffraction studies, although methods exist for achieving large pressure drops in less than 10^{-5} second (19). The need for high-pressure x-ray-transparent windows adds complexity, but not insurmountable difficulties, to the pressure-trigger approach.

Meeting the Diffraction Condition

The generalized reciprocal lattice is the Fourier transform of the specimen electron density distribution. In the case of a perfect single crystal this is the familiar reciprocal lattice. For a perfect powder of the crystal, each reciprocal lattice point is spread onto the surface of a sphere, that is, the ensemble average of all the randomly rotated perfect crystal reciprocal lattices of the microcrystals in the powder. A generalized reciprocal lattice can be defined for any specimen by appropriately averaging over all subunits in the specimen. The distribution of diffracted x-rays may be determined by the Ewald construction (20): for x-rays of wavelength λ construct a sphere of radius $1/\lambda$ (in reciprocal space) such that the origin of the reciprocal lattice is on the surface of the sphere and such that the vector representing the sphere radius to the reciprocal origin is coincident with the incident x-ray momentum vector, \mathbf{k} , where $|\mathbf{k}| = 2\pi/\lambda$. Diffraction of x-rays along a ray projecting out of the Ewald sphere occurs whenever the Ewald sphere and the generalized reciprocal lattice overlap. In this case, the intensity of diffraction grows with the product of the overlap integrated along the ray direction. If the incident radiation is polychromatic, then one imagines a superposition of Ewald spheres, one for each wavelength.

Reconstruction of the specimen electron density, that is, solution of the structure, requires knowledge of the reciprocal lattice. For nonisotropic materials it is often necessary to rotate the specimen relative to the incident beam to cause regions of the reciprocal lattice to intersect the Ewald sphere and, thereby, diffract. This is the usual case in single crystal diffractometry, where the reciprocal lattice points are very small and the Ewald sphere is thin. In a rapid time-resolved experiment, mechanical rotation of the specimen can be very limiting. In the case of SAXS, it is often unnecessary to rotate the sample. For most of the experiments listed in Table 1, because the diffraction angles are small, the Ewald sphere is nearly coincident with the $k_x - k_y$ plane (Fig. 3). Furthermore, all of the SAXS specimens have some degree of disorder that broadens the generalized reciprocal lattice (Fig. 3) such that substantial intersection with the Ewald sphere occurs out to a limiting resolution at a fixed orientation of the specimen. In some sense, mosaic disorder in SAXS specimens is useful in time-resolved experiments because it helps remove the need for rotation of the specimen. The number of x-ray reflections in many SAXS specimens is small (<100), so each reflection can broaden substantially before overlap of reflections becomes a severe problem.

In the case of single protein crystals, however, the desired reciprocal lattice consists of many thousands of sharp points more or less uniformly distributed in reciprocal space. It is necessary to keep the reflections sharp so that they can be uniquely indexed and the individual intensities determined. An alternative strategy to broadening the reciprocal lattice points to intersect the Ewald sphere is to use polychromatic radiation to superimpose Ewald spheres of different radii and create a thickened Ewald "sphere" to perform a Laue diffraction experiment (20). Until the recent work of Moffat and colleagues (9, 21), it was assumed that overlap of reflections of different order would seriously limit interpretation of protein Laue patterns; this turns out not to be the case. Since numerous reciprocal lattice points diffract simultaneously in a polychromatic beam, large fractions [$\sim 70\%$ (22)] of the data up to 3 Å resolution can be recorded in single exposures with a stationary crystal. Limited data are often adequate for the determination of the difference structures needed for time-resolved work.

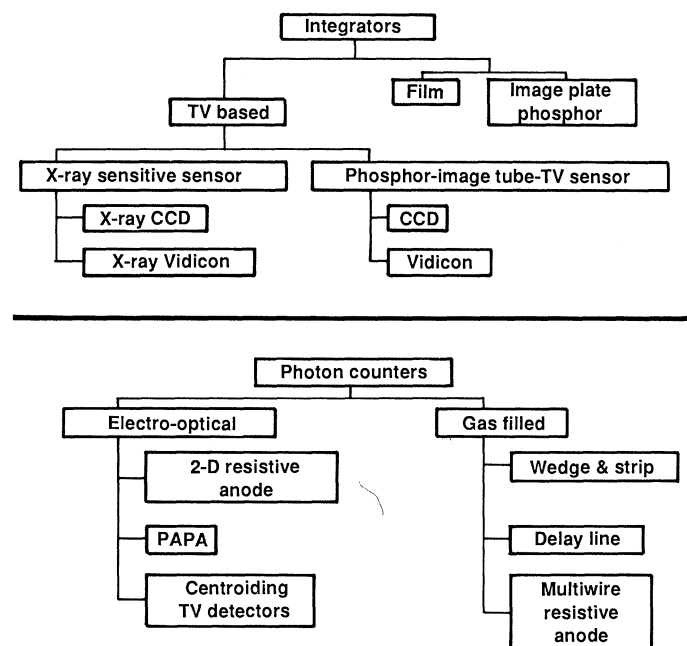


Fig. 4. X-ray detectors may be classed either as integrators or photon counters. Detectors are reviewed in (25) and (26).

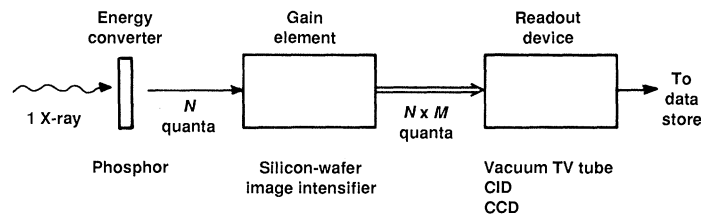


Fig. 5. The basic TV-based two-dimensional x-ray detector typically consists of an energy converter, such as a phosphor, a gain element, such as an image intensifier, which point-by-point amplifies the light, and a TV sensor to accumulate the amplified image. Depending on the particular components and requirements of the detector, a distinct energy converter or gain element may be absent. For example, a bare CCD or charge injection detector (CID) can directly absorb and detect an x-ray pattern with excellent quantum efficiency. [Adapted with permission from (25)]

Laue diffraction of proteins makes possible millisecond and submillisecond exposure times. Tens of millisecond diffraction patterns are already feasible at existing synchrotron sources (9, 21). The technique is one of the more exciting, and potentially powerful, applications of time-resolved diffraction and it is being actively pursued (22–24).

Detectors

The third essential element of the time-resolved diffraction experiment is the x-ray detector [see (25, 26) for recent reviews]. X-ray detectors may be divided into two families: photon counters and integrators (Fig. 4). Photon counters detect x-rays one at a time and allocate information with respect to the x-ray position and, perhaps, time of arrival to digital memory. The classic example is the one-dimensional wire proportional counter. Integrators, by contrast, are exposed to the diffraction pattern for some period of exposure time, after which the signal integrated on each resolution element of the detector is read out. The classic integrator is x-ray film. Photon counters and integrators have qualitatively different limitations when applied to time-resolved diffraction. Photon counters process each x-ray individually; this takes a certain amount of time during which the detector cannot accept another photon in one or more resolution elements. Thus, photon counters suffer from count-rate limitations. Integrators generally expose all resolution elements in parallel and integrate the local x-ray intensity information in analog form. However, periodically the exposure process must be terminated and the recorded information read out or removed. Thus, integrating detectors have duty-cycle limitations. Photon counters operate continuously, but only if the x-rays do not arrive too quickly. Integrators can accept x-rays at very high rates, but only for limited periods of time before the storage medium saturates.

At low count rates, photon counters are very convenient. However, count rates at synchrotron sources rapidly outpace the capabilities of area photon counters. Consider, for example, the case discussed earlier of existing synchrotron sources and typical biological materials, for which the intensities and scattering powers are $10^{10} < I < 10^{16}$ and $10^{-3} < S < 10^{-6}$, respectively. The detector must handle $10^4 < S \times I < 10^{13}$ photons per second. The state of the art in high resolution two-dimensional photon counters is a count rate of less than 10^6 photons per second. At future sources the count-rate problem is worse. Another way of looking at the problem is to consider the data channel that connects the detecting elements to digital memory. To encode the position of an x-ray at reasonable areal resolution, say, to within 512 by 512 resolution elements, requires 14 bits of information (7 bits per coordinate). Even at 10^7 photons per second, this requires a channel capacity of $14 \text{ bits} \times 10^7$

Hz = 17.5 Mbytes per second. At 10^{13} photons per second, this jumps to 17,500 Gbytes per second. Of course, the desired diffraction patterns contain much less than a gigabyte of information. Most researchers performing time-resolved experiments would be satisfied to know the x-ray intensity in each resolution element (512 by 512) to one part in $2.6 \times 10^5 = 2^{18}$ in 100 time slices. This amounts to ~ 0.6 Mbyte of information per time slice or 60 Mbytes for 100 time slices. This illustrates that the enormous channel capacities required from photon counters arise from the data rate, not the amount of data.

This does not imply, of course, that photon counters cannot be of great use in rapid time-resolved experiments. Table 1 indicates they have been used to advantage in instances where the desired information in the diffraction patterns is one-dimensional and most of the diffraction pattern area can be ignored. However, only integrating detectors are capable of operating at the higher count rates when true area detection is desired.

X-ray film is one of the oldest and still one of the most important of the integrating area detectors. Film is inexpensive, has excellent spatial resolution, has large size, and is capable of operating at extremely high count rates. Film is, in some sense, a photon counter in that, as opposed to optically exposed photographic film, each x-ray exposes one film grain. Under a microscope, the exposed, darkened film grains in a piece of developed film are readily counted, although, in practice, film is always read out in analog form by microdensitometry. The disadvantages of film are primarily nonlinearity, high intrinsic noise, narrow dynamic range, and the need for chemical processing. The nonlinearity at high exposures, that is, saturation, results from the overlapping shadows of darkened grains. The high intrinsic noise results from the fluctuation in the number of chemically developed fog grains even at zero x-ray dose. There are $\sim 10^7$ fog grains per square centimeter (27), which has a fluctuation, or noise, of $N = (10^7)^{1/2} \approx 3000$. Thus, an x-ray signal spread out over 1 cm^2 , which exposes less than 3000 grains, readily gets lost in the fog noise. The noise at low dose and saturation at high dose severely limit the useful dynamic range (28). In practice, the dynamic range is extended by stacking films, but this requires scale factors to normalize the different films in the stack.

Storage phosphors appear to be an attractive, newly developing alternative to film (29). A storage phosphor imaging plate (IP) consists of a thin sheet of photostimulable phosphor such as BaFBr:Eu²⁺. X-rays incident upon the IP excite color-centers that have half-lives of many hours. Within this period of time the IP is scanned by means of photostimulated luminescence in a readout device custom built for the process. In photostimulated luminescence, a laser is scanned over the surface of the IP, and excited electrons from the color-center traps are excited into the conduction band; this results in a luminescent signal that is sensed by a photomultiplier. The intensity of the luminescence at each point in the laser scan is a measure of the x-ray dose incident upon that point. The IP (29) has excellent dynamic range (10^6), large size, moderate resolution ($\sim 300 \mu\text{m}$), excellent linearity, very low zero-dose noise (equivalent to 3 x-rays per pixel) and near ideal quantum efficiency up to doses of roughly 10^4 x-rays per $(100 \mu\text{m})^2$. At higher doses, the apparatus limits the accuracy to about 2%. Relative to x-ray film, the major drawbacks of the IP system are the expense of the readout scanner and the poor spatial resolution, both of which are probably a consequence of the fact that the commercial system has been developed for medical radiography.

Imaging plates and film both have the serious disadvantage that the diffraction image must be processed "off-line" and is not immediately available to the experimentalist on the synchrotron floor. By contrast, a variety of television (TV)-based vidicon and charge coupled device (CCD) area x-ray detectors provide a fully

processed image in seconds or milliseconds. TV sensors, having been designed for optical recording, have been subject to much research and development for applications ranging from daylight TV recording ($>10^4$ photons per second per square millimeter) to astronomical imaging (<1 photon per second per square millimeter).

The generic TV detector is shown schematically in Fig. 5. In the most common configuration, the x-ray image is converted to a light image that is, in turn, image intensified before being recorded on the TV sensor. Numerous phosphors, image intensifiers, and TV sensors have been used for x-ray detection, as reviewed elsewhere (25). For the purpose of this article, discussion will be confined to general considerations, devices that have been used in time-resolved diffraction applications, and prospects for the near future.

Efficient inorganic phosphors, such as ZnS(Ag), Gd₂O₂S, Y₂O₂S, and CsI(Na or Tl) convert 5 to 20% of the incident x-ray energy to light. Thus, an 8-keV x-ray yields roughly 100 to 700 isotropically directed optical photons. Given absorption, directional losses in the phosphor, and coupling losses to the next detector element, on the order of 50 to 100 photons are available at the photosensitive surface with 1:1 fiber optical coupling. This number is reduced by a factor of 10 or more if lens coupling is used, which is why lens coupling has not been extensively utilized in applications where the detected x-ray flux is limiting.

Two important numbers that characterize the TV sensors are the saturation level and read-out noise per picture element, or pixel. These numbers vary greatly with the type of TV sensor used. The most important sensors are silicon diode vidicons (30) and silicon CCDs (31), which may be obtained with levels (noise; saturation) of about (5×10^5 ; 10^3) and (5×10^5 ; <10) electrons, respectively. Clearly, CCDs have distinct noise advantages over vidicons. The noise level is also very much a function of the mode of operation of the sensor. The low noise figures given above are obtainable under the cooled, slow-scan read-out mode developed by the astronomy community for recording weak telescope images (30, 32). In this mode, the sensor is read out slowly (1 to 20 seconds) through a narrow bandpass preamplifier so as to exclude much of the noise spectrum associated with video-rate readout. At video rates (30 to 50 frames per second, where 1 frame = 1 full sensor readout) the noise figure of vidicons rises and reduces the available dynamic range per frame so that dynamic ranges of more than 100 are difficult to achieve in practice. At video rates, CCDs also suffer severalfold increased noise but this still leaves considerable dynamic range (10^3 to 10^4).

Most of the development performed to date on quantitative TV-based area x-ray detectors has been done on vidicon sensors for reasons of sensor availability. In the case of vidicons, assuming a $\sim 50\%$ quantum efficiency of converting optical photons to usable electron-hole pairs, 100 optical photons per 8-keV x-ray (see above), and slow-scan noise of $\sim 10^3$ electrons per pixel, one sees that each x-ray, at best, contributes a signal-to-noise ratio of $(10^2 \times 0.5)/10^3 = 0.05$. Thus, at low dose, the detector noise dominates the image statistics. For this reason, image intensifiers are usually interposed between the phosphor and the TV sensor. Image intensifier photocathodes have quantum efficiencies of about 10 to 20%, so each x-ray yields about 5 to 15 photoelectrons per x-ray (33). As long as the number of photoelectrons per x-ray is significantly larger than unity, then, for phosphors that stop most of the incident x-rays, the fluctuations in the photoelectron number will be dominated by the shot noise of the incident x-ray signal. Low noise, multistage image intensifiers with optical gains up to $\sim 10^6$ are available, so there is no difficulty providing sufficient visible light photons to the vidicon sensor such that the signal per incident x-ray is well above the readout noise. In these cases, the overall noise even

at low dose is dominated by the incident x-ray photon statistics and the detector is said to be "quantum limited."

The much lower noise of CCDs means that the phosphor light from each stopped x-ray can directly excite the CCD and still provide more signal than the readout noise per pixel, at least for a 1:1 magnification of the phosphor image. Unfortunately, CCD and vidicon sensors are small (1 to 2 cm in diameter), considerably smaller than most diffraction patterns. This often necessitates image demagnification, which reduces the light transferred to the sensor by a factor that shrinks at least as fast as the square of the demagnification (34). Thus, image intensifiers are often necessary even in the case of CCDs simply to reduce the format of the image. Details of the noise factors and coupling efficiencies for various configurations are discussed by Deckman and Gruner (34).

Three comments are useful here with respect to future detectors. First, large area (5 by 5 cm), high resolution (2048 by 2048 pixels) prototype CCDs have been produced (35). Second, many diffraction experiments can be scaled down in size as, for example, by the use of shorter wavelength x-rays, or by the use of small specimens and short specimen to detector distances. The lower limit of size of a diffraction spot is given by the overlap area of the specimen in the beam, since this area is convolved in the diffraction pattern with the ideal diffraction pattern expected for an infinitesimal point source. As the x-ray source brightness increases, the study of micrometer size specimens become feasible (10). Impetus in this direction will also come from the fact that small (10 to 50 μm across) protein crystals are much more readily obtainable than large (200 μm in diameter) crystals. Problems of heating and radiation damage for protein microcrystals have been discussed (12). For a 20- μm specimen, one can envision a quantum-limited detector suitable for reduced-scale experiments, consisting of a phosphor directly coupled by 1:1 fiber optics to a CCD. Elimination of the image intensifier is desirable since image tube systems are expensive and complex, and since the image intensifier generally degrades the spatial resolution of the final image. Third, CCDs are directly x-ray sensitive and are capable of acting as high quantum efficiency sensors without intervening phosphors (36). However, radiation damage at high x-ray doses is likely to limit the usefulness of current devices. Radiation-hardened semiconductors can be constructed.

Film, image plates, and slow-scan TV detectors generally require x-ray shutters to gate the x-rays on during the exposure interval and off during the plate removal or detector read-out period. Continuously scanned TV detectors operating, for instance, at video rates circumvent this difficulty as long as the brightness of the diffraction pattern is insufficient to saturate the video-rate dynamic range of the TV sensor during the ~ 30 -msec scan period. In its simplest configuration such a system consists of a phosphor-image intensifier unit lens coupled to a commercial video-rate TV camera with the results recorded on video tape. Although such a system is far from ideal, it has three extremely important attributes: it is inexpensive, simple, and readily assembled from off-the-shelf components. Caffrey at Cornell has used such a system to examine phase transitions in lipid liquid crystals [Table 1 and (15)].

The wider dynamic range and lower noise of custom assembled video-rate CCD cameras makes them attractive for continuous recording of diffraction images. The reduction of this technology to practice will entail solutions of difficult, although by no means insurmountable, engineering problems: For example, low persistence, intagliated phosphors (37) may be required to simultaneously maintain high spatial resolution and high x-ray stopping power. Analog-to-digital converters operating at 10 MHz with 14 to 16 bits will be required. Finally, mass memory operating at 15 Mbytes/sec will be required to store the images emanating from the detector.

Many detector technologies are suitable for recording two-

dimensional x-ray patterns at low count rates. Although photon counting instruments saturate at the high count rates inherent in many time-resolved diffraction experiments, integrating detectors such as film, image plates, and slow scan TV-based systems appear capable of recording at the highest projected count-rates. Fast-scan vidicon based systems have limited dynamic range (~ 100), which seriously limits their capabilities for time-resolved work faster than the ~ 0.03 -sec frame read-out time. It appears likely that fast-scan CCDs can operate with dynamic ranges of 10^3 to 10^4 , although such detectors have yet to be developed. Historically, detector development has lagged behind x-ray source development. It may be anticipated that pressure for rapid detector development will build as bright synchrotron sources become available. Since both image plate and CCD detectors are new and extremely promising technologies, improvements in the already impressive capabilities of these detectors are to be expected. Most importantly, significant engineering must be done before the current laboratory prototypes become useful instruments at user facilities.

Conclusion

Numerous biological processes proceed on millisecond time scales, yet very few of these have been structurally examined in time-resolved fashion. Although I have emphasized that millisecond diffraction is accessible with existing technology, such diffraction is still extraordinary, with very few studies having been performed on these time scales. The reason so few studies have been performed is simply that obtaining properly configured x-ray beam lines, specimens, and detectors in the same place at the same time is still a formidable task. Of the three essential components, suitable beam lines are most readily available. Detector development has lagged considerably. Suitable slow-scan TV detectors are rarely available at high brightness, tightly focused beam lines. Where electronic area detectors do exist, they tend to be either count rate-limited or of low dynamic range. Image plate systems are just beginning to be installed. Without routine access to suitable beam lines and detectors, there has been relatively little impetus to explore specimen configurations and triggers. This situation will change in the future, but it should be recognized that the rate of change will largely be a function of the demands and participation of the community interested in biological materials.

REFERENCES AND NOTES

1. H. Winick and S. Doniach, *Synchrotron Radiation Research* (Plenum, New York, 1980); also, many articles in *Synchrotron Radiation Instrumentation*, G. S. Brown and I. Lindau, Eds., *Nucl. Instrum. Methods A246*, 1 (1986).
2. Entries in Table 1 are chosen for illustrative purposes only. This article is not intended as a review, since the literature on time-resolved diffraction is already too large to be comprehensively reviewed in an article of this kind.
3. A. Franks, *Proc. Phys. Soc. London, Sect. B* **68**, 1054 (1955).
4. See, for instance, *Small Angle X-ray Scattering*, O. Glatter and O. Kratky, Eds. (Academic Press, New York, 1982).
5. M. Caffrey and D. H. Bilderback, *Nucl. Instrum. Methods* **208**, 495 (1983).
6. N. F. Gmur and S. M. White-Depace, Eds., *National Synchrotron Light Source Users Manual* (Brookhaven National Laboratory, Upton, NY, 1986).
7. M. W. Tate, S. M. Gruner, E. Shyamsunder, K. L. D'Amico, *Bull. Am. Phys. Soc.* **32**, 843 (1987).
8. J. R. Helliwell, *Rep. Prog. Phys.* **47**, 1403 (1984).
9. See references in D. H. Bilderback, K. Moffat, D. M. E. Szebenyi, *Nucl. Instrum. Methods* **222**, 245 (1984).
10. B. Hedman, K. O. Hodgson, J. R. Helliwell, R. Liddington, M. Z. Papiz, *Proc. Natl. Acad. Sci. U.S.A.* **82**, 7604 (1985).
11. P. Eisenberger, *Science* **231**, 687 (1986); B. Buras and G. Materlik, *Nucl. Instrum. Methods A246*, 21 (1986).
12. See worked examples in J. R. Helliwell and R. Fourme, "European Synchrotron Radiation Project Report ESRP-IRI-4/83" (CERN, Geneva, 1983); W. A. Hendrickson *et al.*, "Report on the Workshop on the Scientific Case of 6 GeV Synchrotron Source" (Department of Energy, Washington, DC, December 1985).
13. R. D. Frankel and J. M. Forsyth, *Biophys. J.* **47**, 387 (1985).

14. B. C. Larson, C. W. White, T. S. Noggle, J. F. Barhorst, D. M. Mills, *Appl. Phys. Lett.* **42**, 282 (1983).
15. M. Caffrey, *Biochemistry* **24**, 4826 (1985).
16. J. K. Blasie *et al.*, *Biophys. J.* **48**, 9 (1985).
17. J. A. McCray, L. Herbert, T. Kihara, D. R. Trentham, *Proc. Natl. Acad. Sci. U.S.A.* **77**, 7237 (1980).
18. Time-resolved muscle diffraction studies are reviewed by H. E. Huxley and A. R. Faruqi, *Annu. Rev. Biophys. Bioeng.* **12**, 381 (1983).
19. J. S. Davis and H. Gutfreund, *FEBS Lett.* **72**, 199 (1976).
20. See, for instance, A. J. C. Wilson, *Elements of X-ray Crystallography* (Addison-Wesley, Reading, MA, 1970).
21. K. Moffat, D. Szebenyi, D. Bilderback, *Science* **223**, 1423 (1984); K. Moffat, D. Bilderback, W. Schildkamp, K. Volz, *Nucl. Instrum. Methods* **A246**, 627 (1986).
22. J. Hadju *et al.*, *EMBO J.* **6**, 539 (1987).
23. K. Moffat, D. Szebenyi, W. Schildkamp, D. Szebenyi, R. Loane, in *Structural Biological Applications of X-ray Absorption, Scattering and Diffraction*, B. Chance and H. Bartunik, Eds. (Academic Press, New York, 1986); J. R. Helliwell, *J. Mol. Struct.* **130**, 63 (1985).
24. M. Harding, S. Maginn, P. Machin, J. Campbell, I. Clifton, *Daresbury Lab. Inf. Q. Protein Cryst.* **19**, 43 (1986).
25. S. M. Gruner, J. R. Milch, G. T. Reynolds, *Nucl. Instrum. Methods* **195**, 67 (1982).
26. U. W. Arndt, *J. Appl. Crystallogr.* **19**, 145 (1986).
27. D. W. Smits and E. H. Wiegenga, *Acta Crystallogr.* **9**, 520 (1956); H. Morimoto and R. Uyeda, *ibid.* **16**, 1107 (1963).
28. The dynamic range may be defined in many ways. For the purposes of this article it is defined as the ratio of the saturated signal to the root-mean-square noise per resolution element, or pixel, per frame readout. See S. M. Gruner, J. R. Milch, G. T. Reynolds, *IEEE Trans. Nucl. Sci.* **NS-25**, 562 (1978); S. M. Gruner and J. R. Milch, *Trans. Am. Crystallogr. Assoc.* **18**, 149 (1982).
29. J. Miyahara, K. Takahashi, Y. Amemiya, N. Kamiya, Y. Satow, *Nucl. Instr. Methods* **A246**, 572 (1986); Y. Amemiya, K. Wakabayashi, H. Tanaka, Y. Ueno, J. Miyahara, *Science* **237**, 164 (1987); K. Moffat *et al.*, *Nucl. Instrum. Methods*, in press; B. R. Whiting, J. F. Owen, B. H. Rubin, *ibid.*, in press.
30. P. Crane and M. Davis, *Publ. Astron. Soc. Pac.* **87**, 207 (1975).
31. J. A. Hall, in *Applied Optics and Optical Engineering*, R. R. Shannon and J. C. Wyant, Eds. (Academic Press, New York, 1980), vol. 8.
32. See, for example, J.-P. Baluteau and S. D'Odurico, Eds., *The Optimization of the Use of CCD Detectors in Astronomy*, conference and workshop proceedings, No. 25 (European Southern Observatory, Munich, 1986).
33. J. H. Chappell and S. S. Murray, *Nucl. Instrum. Methods* **221**, 159 (1984).
34. H. W. Deckman and S. M. Gruner, *ibid.* **A246**, 527 (1986).
35. Tektronix model TK2048M (Tektronix, Inc., Beaverton, OR 97077).
36. R. E. Griffiths, *Adv. Electron. Electron Phys.* **64B**, 483 (1985); D. H. Lumb, G. R. Hopkinson, A. A. Wells, *ibid.*, p. 497.
37. V. Duchenois, M. Fouassier, C. Piaget, *ibid.*, p. 365.
38. H. E. Huxley, A. R. Faruqi, J. Bordas, M. H. J. Koch, J. R. Milch, *Nature (London)* **284**, 140 (1980).
39. G. Suarez *et al.*, *Proc. Natl. Acad. Sci. U.S.A.* **82**, 4693 (1985).
40. J. Bordas, E.-M. Mandelkow, E. Mandelkow, *J. Mol. Biol.* **164**, 89 (1983).
41. A. Mahendrasingam *et al.*, *Science* **233**, 195 (1986).
42. G. Mulhaupt, *Nucl. Instr. Methods* **A246**, 845 (1986).
43. I am grateful to U. Arndt, D. Bilderback, M. Caffrey, S. Doniach, P. Eisenberger, K. Hodgson, H. Huxley, K. Moffat, G. T. Reynolds, and D. Ringe for comments and references. Biomedical research and instrumentation development in our laboratory is supported by NIH grant GM32614, and DOE grant DE-FG02-87ER60522.A000. Instrumentation development for beam line X-9 at the NSLS is supported by NSF grant PCM 8313069. Research at NSLS beam line X-10 is also supported in part by Exxon Research & Engineering Co.

New Opportunities in Synchrotron X-ray Crystallography

C. T. PREWITT, P. COPPENS, J. C. PHILLIPS, L. W. FINGER

Several high-intensity synchrotron x-ray sources have been constructed over the past few years in the United States, West Germany, Great Britain, Japan, France, Italy, and the Soviet Union. Crystallographers have begun to use these facilities for experiments that take advantage of the characteristics of synchrotron radiation, namely, a broad distribution of wavelengths, high intensity, low divergence, strong polarization, and a pulsed time structure. In addition to more familiar diffraction experiments on single crystals and powdered samples, new types of crystallographic studies, for example, energy-dispersive and surface diffraction studies, have progressed rapidly with more general accessibility of synchrotron sources. These high-intensity sources allow diffraction experiments to be performed on very small crystals or on large biological molecules, and permit weak magnetic scattering to be detected. Anomalous dispersion experiments can exploit the ability to vary the wavelength of the radiation, and the pulsed time structure of the beam makes possible fast time-resolved experiments. Because of the availability of synchrotron x-radiation, these and other kinds of experiments will be in the forefront of crystallographic research for the next several years.

THE TRADITIONAL SOURCE OF INCIDENT RADIATION FOR X-ray diffraction experiments has been an evacuated tube that contains a cathode and anode that is subjected to a high electrical potential. These tubes have been incorporated into a variety of instruments found in laboratories all over the world. In recent years, however, crystallographers have been presented with an extraordinary opportunity resulting from the construction of several high-intensity synchrotron x-ray sources in the United States, West Germany, Great Britain, Japan, France, Italy, and the Soviet Union. Synchrotron radiation results when high-energy electrons are accelerated in the magnetic fields required to close the orbits in storage rings or synchrotrons; for the facilities discussed here, the radiation can have energies ranging from the x-ray into the infrared regions. A typical installation consists of a linear electron accelerator from which electrons are injected at a relatively high energy into a storage ring several tens of meters in diameter. Such a ring consists of straight and curved sections. Electrons are guided around this ring with a series of magnets, and accelerating fields are supplied by one or more radio-frequency (rf) stations located at

C. T. Prewitt and L. W. Finger are at the Geophysical Laboratory, Carnegie Institution of Washington, 2801 Upton Street, NW, Washington, DC 20008. P. Coppens and J. C. Phillips are at the Department of Chemistry, State University of New York, Buffalo, NY 14214. J. C. Phillips is also associated with the SUNY X3 beamline, National Synchrotron Light Source, Brookhaven National Laboratory, Upton, NY 11973.